CO_2-driven stratocumulus cloud breakup in a bulk boundary layer model

Clare E. Singer[1] and Tapio Schneider[1]

[1]California Institute of Technology

April 16, 2023

CO_2-driven stratocumulus cloud breakup in a bulk boundary layer model

Clare E. Singer[a] and Tapio Schneider[a]

[a] *California Institute of Technology, Pasadena, California*

Corresponding author: Clare E. Singer, csinger@caltech.edu

ABSTRACT: Stratocumulus clouds cover 20% of subtropical oceans and strongly cool the Earth by reflecting incoming shortwave radiation. Because of their small dynamical scales and their sensitivity to changing meteorological conditions, the response of stratocumulus clouds to climate change is one of the leading uncertainties in climate modeling. Recent work has made significant progress constraining this feedback using high-resolution large eddy simulations (LES) and satellite observations. Here we provide complementary constraints from a theoretical perspective, using a bulk boundary layer model to calculate the response of stratocumulus clouds to increasing CO_2. We extend the bulk model presented in Singer and Schneider (2023) by coupling it to a slab ocean to allow for feedbacks between cloud cover and surface warming and use ensemble Kalman inversion to calibrate model parameters. We conduct climate change experiments, forcing the bulk model with increasing CO_2, and compare the cloud response to results from LES in Schneider et al. (2019). Past a critical CO_2 value, the cloud layer decouples from the surface, the clouds break up, and cloud fraction decreases to a shallow cumulus-like state. Cloud fraction shows hysteresis behavior, where the system remains in a low cloud fraction state even as CO_2 is decreased significantly past the breakup threshold. The hysteresis behavior is robust, but the critical CO_2 value is sensitive to parameters and assumptions of the bulk model. We show that surface warming and water vapor feedback are two important aspects of the breakup; without them, the critical CO_2 threshold for breakup is much larger.

SIGNIFICANCE STATEMENT: The purpose of this study, and the companion paper Singer and Schneider (2023), is to develop a simple model to explain mechanisms controlling stratocumulus-cumulus transitions. In this second paper, we describe the extended bulk model coupled to a slab ocean that is forced only with a prescribed CO_2 concentration. We calibrate key parameters of this model based on high-resolution simulations. The simple model, like the high-resolution simulations, shows that stratocumulus clouds break up at very high CO_2 concentrations and that the boundary layer exhibits hysteresis, remaining in a cumulus-like state until CO_2 is reduced significantly past the breakup threshold. We conclude by showing a series of mechanism-denial experiments that highlight the importance of surface temperature and water vapor feedbacks on the stratocumulus breakup.

1. Introduction

The response of stratocumulus clouds to increasing CO_2 has been an outstanding question in the field for the past several decades; it remains one of the largest contributors to uncertainty in warming and equilibrium climate sensitivity (ECS) (Sherwood et al. 2020; Zelinka et al. 2022). Global climate models (GCMs) exhibit a large spread in predictions of changes in low clouds, which percolates into a large spread in ECS. GCMs struggle to model low clouds, in particular stratocumulus, because of the small dynamical scales relevant for cloud-scale turbulence (~ 10 m) compared to the coarse resolution of models (~ 100 km) (Schneider et al. 2017). The result is inaccurate simulation of the present-day climate, with radiative biases on the order of 10 W m^{-2} and more in subtropical stratocumulus regions, and a large spread of model responses to CO_2 perturbations (Nam et al. 2012; Brient et al. 2019). Increasing resolution of models, even into convection-permitting regimes, can only help improve stratocumulus to a certain extent (Lee et al. 2022).

To get around this shortcoming of GCMs, some recent studies have taken the approach of using satellites to measure co-variability between clouds and meteorology to observationally constrain cloud feedbacks and ECS (e.g., Brient and Schneider 2016; Cesana and Del Genio 2021; Myers et al. 2021; Ceppi and Nowack 2021). Other studies, such as the CGILS project (Zhang et al. 2012; Blossey et al. 2013; Bretherton et al. 2013) and Tan et al. (2017), have explored low-cloud

responses to CO_2 in large-eddy simulations (LES), where the most energetic small-scale motions are directly resolved. Bretherton (2015) summarizes results from such LES studies.

However, given the shortcomings of GCMs in simulating clouds, and the difficulty of interpreting LES without a clear and quantitative conceptual framework, advances in theory are necessary for progress on the cloud problem. In this paper, we present a bulk boundary layer model for stratocumulus-topped boundary layers that includes a very simple radiative transfer scheme and is coupled to a slab ocean surface. We build on previous work by Deardorff (1980), Lilly (1968), Bretherton and Wyant (1997), Stevens (2006), Dal Gesso et al. (2014), and de Roode et al. (2014). Our purpose is to provide a conceptual bridge to go between LES and GCMs and a framework for understanding and interpreting both. Specifically, we build a conceptual model to interpret the LES of Schneider et al. (2019), who simulated a stratocumulus-topped boundary layer under different CO_2 conditions. They concluded that eventually, at very high CO_2, the increased infrared opacity of the free troposphere will shut down the critical cloud-top longwave cooling that drives the sustaining overturning circulation in the boundary layer, leading to stratocumulus cloud breakup. The primary mechanism for the stratocumulus breakup is the "direct effect" of CO_2 on the cloud-top radiative cooling. CO_2 was only recently recognized as an important driver of this direct reduction in cloud-top longwave cooling (Bretherton et al. 2013; Tan et al. 2017; Schneider et al. 2019, 2020), but other radiative drivers such as high clouds and water vapor, which both alter the downwelling longwave radiation at cloud-top have been noted previously (Christensen et al. 2013). The direct effect of CO_2 on cloudiness has also been recently noted as an important mechanism to explain the observed TOA energy imbalance in the historical satellite record (Raghuraman et al. 2021). Our bulk model provides a conceptual basis for quantitative analysis and interpretation of this direct effect, among other factors affecting cloud cover.

The paper is organized as follows: Section 2 describes the bulk boundary layer model coupled to a slab ocean. Section 3 discusses calibration of bulk model parameters. Section 4 discusses stratocumulus break-up mechanisms, presenting results from the bulk model and comparing them to LES from Schneider et al. (2019), and explores sensitivities of the results to the calibrated parameters. Section 5 summarizes the conclusions.

2. Bulk boundary layer model with interactive SSTs

Singer and Schneider (2023) describe the derivation of bulk boundary layer model with prescribed boundary conditions. The following section describes a further extension. First we couple the atmospheric boundary layer to a slab-ocean by adding a prognostic equation for sea surface temperature (SST), and we add an analytical radiative transfer formulation. Then we embed the stratocumulus "box" into a two-column framework (Pierrehumbert 1995; Miller 1997) and parameterize the coupling between the subtropics and tropics.

a. Specifying top and bottom thermodynamic boundary conditions

With a goal to study stratocumulus cloud feedbacks, we need to build a model where the boundary conditions are consistently solved for based on a prescribed value for CO_2. We couple the atmospheric boundary layer to a slab ocean through a surface energy balance to consistently represent surface warming due to increasing CO_2 and to include the positive feedback between cloud thinning and surface warming.

The bulk model is then defined by the following system of five coupled ordinary differential equations:

$$\frac{dz_i}{dt} = w_e - Dz_i + w_{\text{vent}}, \tag{1a}$$

$$\frac{ds}{dt} = \frac{1}{z_i}\left[V(s_0 - s) + w_e(s_+ - s) - \Delta R\right] + s_{\text{exp}}, \tag{1b}$$

$$\frac{dq_t}{dt} = \frac{1}{z_i}\left[V(q_{t,0} - q_t) + w_e(q_{t,+} - q_t)\right] + q_{\text{exp}}, \tag{1c}$$

$$\frac{d\text{CF}}{dt} = \frac{\text{CF}' - \text{CF}}{\tau_{\text{CF}}}, \tag{1d}$$

$$C\frac{d\text{SST}}{dt} = \text{SW}_{\text{net}} - \text{LW}_{\text{net}} - \text{LHF} - \text{SHF} - \text{OHU}. \tag{1e}$$

Equations (1a) – (1d) are the same as Singer and Schneider (2023). The cloud-top radiative cooling, ΔR, is a function of the CO_2 and H_2O above the cloud (Singer and Schneider (2023), their Eqs. 8 and 9). The cloud fraction is parameterized as a relaxation to the diagnosed state CF′ which

depends on the decoupling parameter $\mathscr{D} = (\mathrm{LHF}/\Delta R) \cdot ((z_i - z_b)/z_i)$:

$$\mathrm{CF}' = \mathrm{CF}_{\max} - \frac{\mathrm{CF}_{\max} - \mathrm{CF}_{\min}}{1 + \frac{1}{9}\exp(-m(\mathscr{D} - \mathscr{D}_c))}.$$

For this application, to be consistent with the Schneider et al. (2019) LES, we set $\mathrm{CF}_{\max} = 100\%$ and $\mathrm{CF}_{\min} = 20\%$.

Equation (1e) is the standard surface energy budget equation for SST. On the left-hand side, $C = \rho_w c_w H_w$ is a heat capacity per unit area, where ρ_w and c_w are the density and specific heat capacity of water and H_w is the depth of the slab ocean. The value of H_w is arbitrary: it affects the equilibration time, but not the equilibrium results, which are the object of interest here. We choose $H_w = 1$ m, which gives an equilibration timescale of $\tau_{\mathrm{SST}} \approx 50$ days. On the right-hand side are the source terms from shortwave and longwave radiation, latent and sensible heat fluxes, and ocean heat uptake (OHU).

1) Closed surface energy budget: parameterized surface radiation

The net surface shortwave radiation is simplified to be linear in cloud fraction,

$$\mathrm{SW}_{\mathrm{net}} = a_{\mathrm{SW}} + b_{\mathrm{SW}}(\mathrm{CF}_{\max} - \mathrm{CF}), \tag{2}$$

with coefficients $a_{\mathrm{SW}} = 120$ W m^2 and $b_{\mathrm{SW}} = 140$ W m^2. The net longwave radiation is taken to be a constant $\mathrm{LW}_{\mathrm{net}} = -30$ W m^{-2}, consistent with LES results from (Schneider et al. 2019).

The ocean heat uptake (OHU) is determined as the residual from a steady-state simulation with 400 ppmv CO_2 in which the SST is fixed to 290 K. The OHU is kept fixed across the range of CO_2 concentrations considered (OHU = -12 W m^{-2}).

2) Large-scale circulations: parameterized above-cloud temperature

Reduction of subtropical cloud cover will increase TOA radiative imbalance locally and lead to energy export to the rest of the globe. Some of this energy will be exported to the tropics, warm the tropical free troposphere, and because of weak temperature gradients, feed back and warm the subtropical free-troposphere above the cloud layer (Figure 1). Simplifying the procedure of Schneider et al. (2019), we parameterize the effect of subtropical albedo changes on above-

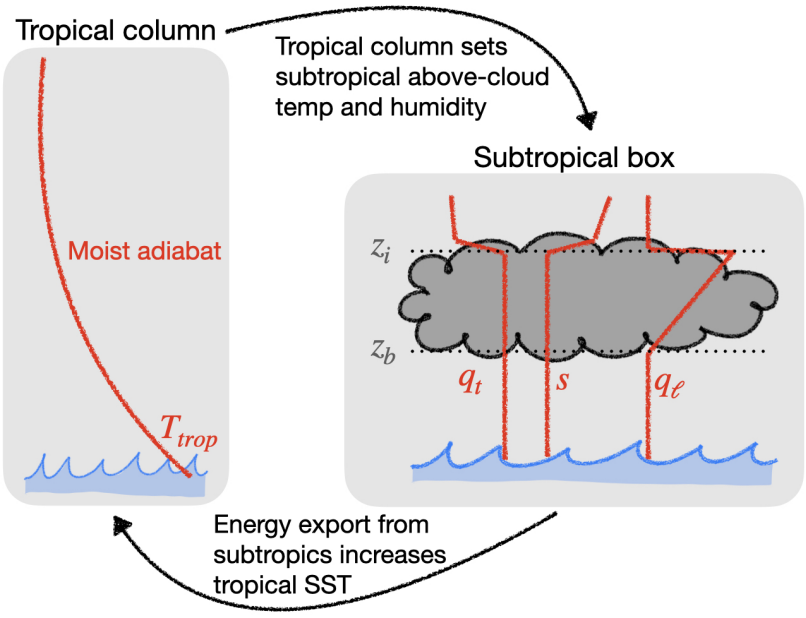

FIG. 1. Schematic of coupling between subtropical domain and tropical domain. Energy is assumed to be exported from the tropics globally when cloud cover decreases; this warms the tropics, and in turn, warms the overlying free-troposphere above the subtropical clouds. This is parameterized by Equation 3.

cloud temperatures by considering how both the direct warming from CO_2 as well as the additional warming from increased subtropical energy export change the strength of the temperature inversion in the subtropics. The inversion strength (IS) is modeled as

$$\Delta_+ T = a_T + b_T \log_2\left(\frac{\mathrm{CO}_2}{400}\right) - c_T(\mathrm{CF}_{\max} - \mathrm{CF}), \tag{3}$$

where $a_T = 8$ K is the IS in the base climate, $b_T = 1.5$ K describes the relative warming in the tropics versus subtropics per doubling of CO_2, and $c_T = 10$ K measures the strength of the energy export into the tropics from subtropical cloud thinning.

3. Ensemble Kalman inversion for parameter calibration

The bulk model as described in Section 2 includes three principal free parameters: The surface exchange velocity $V \equiv C_d U$, the coefficient of ventilation mixing strength α_{vent} (Singer and Schneider (2023), their Eq. 7), and the surface SW cloud radiative feedback strength b_{SW}. Other free

parameters, such as a_{SW} and a_T, are not included in the calibration, and are instead determined independently from the Schneider et al. (2019) LES results. We calibrate the parameters to minimize mismatch between the bulk model results and the LES from Schneider et al. (2019). The quantitative results of the model are sensitive to these exact parameter values; this is explored in detail in at the end of Section 4.

The values of these parameters have physical meaning and are constrained (by the assumed priors) to take on physically reasonable values based on external constraints (such as positivity or order-of-magnitude estimates for maximum ventilation velocities) or previous measurements/studies (order of magnitude for surface exchange velocity). Our parameter priors are Gaussian (Table 1).

Parameter [units]	**Prior**	**Optimal value**
V [m s^{-1}]	$\mathcal{N}(8,2)\times10^{-3}$	7.9×10^{-3}
α_{vent} [m s^{-1}]	$\mathcal{N}(1.2,0.3)\times10^{-3}$	1.69×10^{-3}
b_{SW} [W m^{-2}]	$\mathcal{N}(150,40)$	140

TABLE 1. Table of parameters calibrated, their assumed prior ranges, and the optimal value to which the Ensemble Kalman inversion converges.

We use Ensemble Kalman inversion (EKI), a flexible gradient-free optimization method (Schillings and Stuart 2017), to calibrate these parameters. EKI is an adaptation for parameter estimation of the ensemble Kalman filter, which has been widely used in the atmospheric sciences for state estimation (Houtekamer and Zhang 2016). EKI is robust to noisy data or models with sharp or discontinuous gradients (Lopez-Gomez et al. 2022). We use the `EnsembleKalmanProcesses.jl` Julia implementation of EKI (Dunbar et al. 2022).

Our data in the loss function are domain-mean, time-mean SSTs and LHFs from LES in statistical steady states across a range of CO_2 concentrations both with increasing and decreasing CO_2 from (Schneider et al. 2019). The data covariance matrix is taken to be diagonal, assigning 10% error to each data point, with error reduced to 0.5% for the two endpoints of the up- and down-steps at 1600 ppmv and 200 ppmv, respectively, to put 20x greater weight and ensure the optimization converges on a solution that retains the hysteresis behavior, even at the expense of possible better quantitative accuracy at intermediate CO_2 concentrations. Our loss function is the L_2-norm of the SST and LHF mismatch, both normalized by the mean and standard deviation across the LES simulations.

To calibrate the three parameters, we choose an ensemble size of 90 particles and iterate 15 times until convergence (Figure 2). One evaluation of the forward model consists of evaluating the steady-state result in the bulk model at 17 CO_2 levels, increasing from 200 ppmv to 1600 ppmv and then back down to 200 ppmv. With each successive iteration, the collection of particles

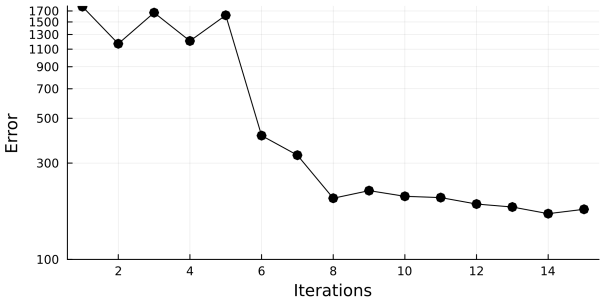

FIG. 2. Error from EKI loss function for each iteration of the parameter optimization. As the particle ensemble collapses towards the optimal values the error decreases. Convergence happens after about 8 iterations.

collapses toward the optimal parameter values (Figure 3). The scatter plots show particles in each 2-dimensional space, and the histograms show the distribution of particles along each parameter dimension separately, with the initialized ensemble (sample from prior) in grey and the final ensemble in red.

The optimal parameter values (mean of all particles at final iteration) are given in Table 1. The predicted SSTs and LHFs from the bulk model using the optimal calibrated parameters is shown compared to the LES results in Figure 4. Some particles in the final ensemble have cloud break up at values above or below 1300 ppmv (not shown). Similarly for the re-formation of stratocumulus at lower values of CO_2, some particles in the ensemble, despite having very similar parameter values, show clouds not reforming, while most show clouds reforming at 400 ppmv. This sensitivity to parameter choices is discussed further in Section 4b.

4. Results

a. Stratocumulus breakup mechanisms

As was identified in the LES experiments from Schneider et al. (2019), at very high concentrations of CO_2, the stratocumulus clouds become unstable and break up into cumulus-like state with low cloud fraction. In our simplified bulk model, we reproduce this behavior (Figure 4).

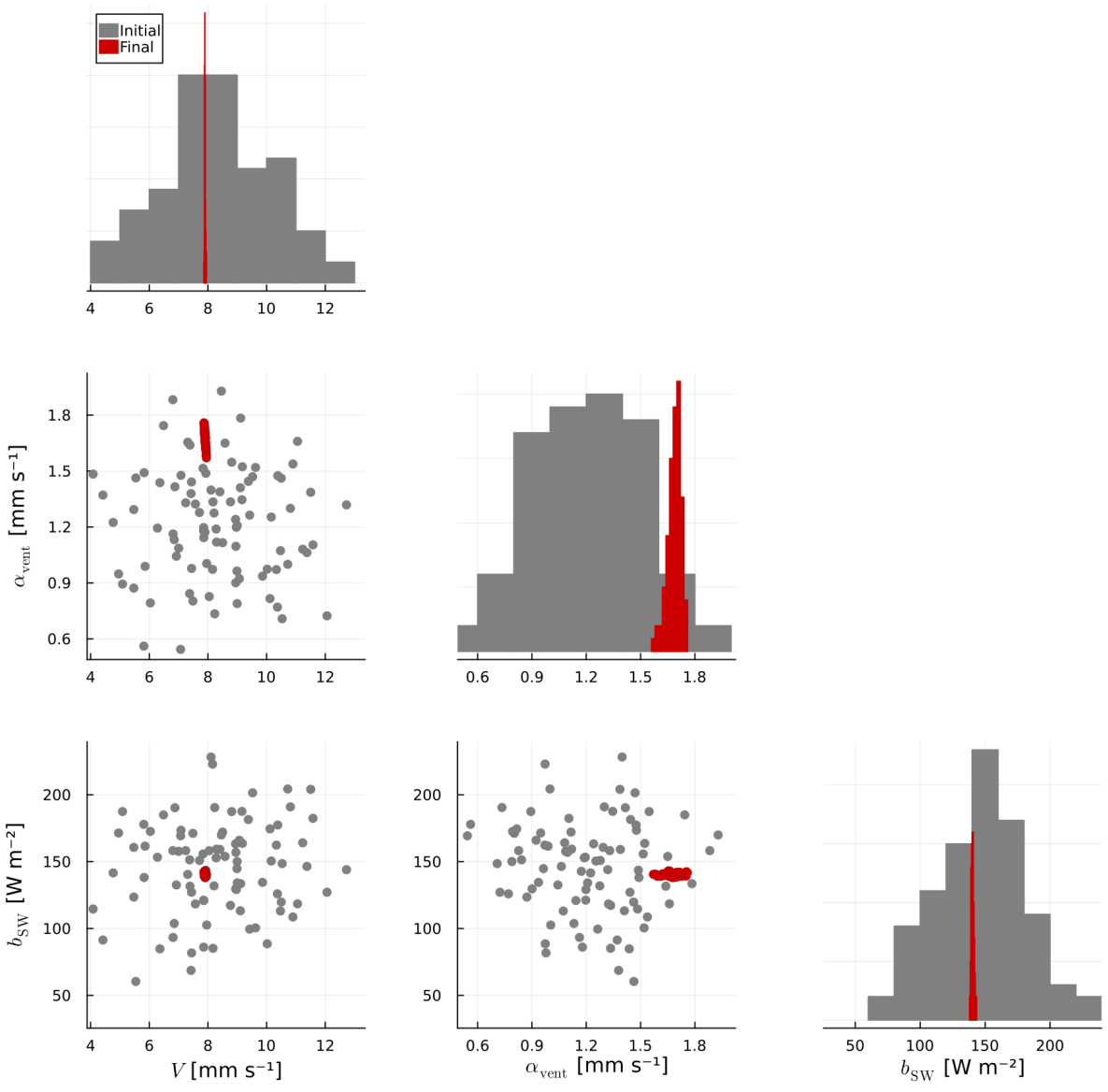

FIG. 3. Plots of initialized (grey) and converged (red) particle ensembles. Scatter plots in the lower left of the figure show the distribution of particles in each 2-dimensional parameter space. Histograms on the diagonal show the distribution of particles in each parameter-dimension individually. Covariance between parameters is weak as indicated by the spread in red points mostly horizontal or vertical, not diagonal. The ventilation mixing strength parameter α_{vent} shows the largest variability in the final ensemble compared to the prior range.

We conduct the same experiment as presented in Schneider et al. (2019). The bulk model is sequentially run to equilibrium at various CO_2 concentrations, starting from 200 ppmv, increasing

to 1800 ppmv, and then decreasing back to 200 ppmv. Each sequential simulation is initialized from the steady-state condition at the previous CO_2 level. In Figure 4, the red points indicate simulations where CO_2 was increased from the previous steady-state solution, and blue points indicate simulations where CO_2 was decreased. Following the red points, we see that the cloud deck

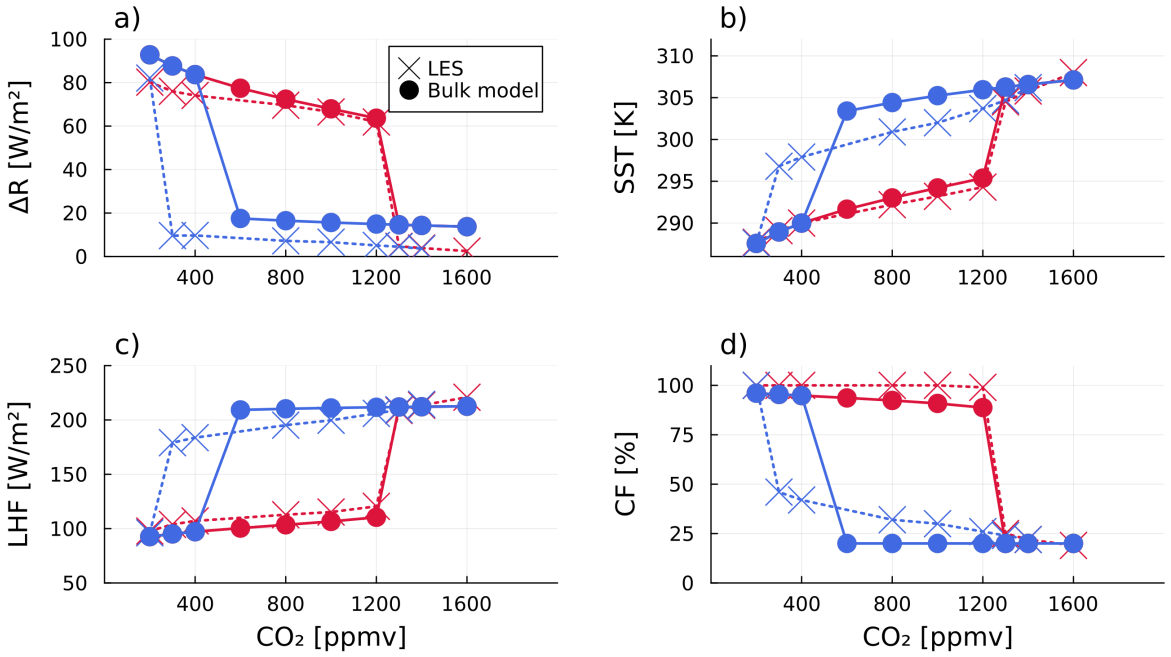

FIG. 4. Steady-state solutions from the bulk model and LES for an experiment of sequentially increasing and then decreasing CO_2 concentrations. Simulations initialized from a lower CO_2 steady-state condition (increasing CO_2) are shown in red, and those initialized from a higher CO_2 state (decreasing) are shown in blue. Panels show (a) the cloud-top radiative cooling, ΔR, (b) sea surface temperature, SST, (c) surface latent heat flux, LHF, and (d) cloud fraction, CF. Results from the bulk model are shown in circles (solid lines) with results from the Schneider et al. (2019) LES shown in crosses (dotted lines).

remains stable up until 1200 ppmv CO_2, but when CO_2 is increased to 1300 ppmv, the stratocumulus deck dissipates (Figure 4d). Coincident is a rapid warming of sea surface temperatures (Figure 4b). As CO_2 is decreased from the maximum value simulated (1800 ppmv), the blue points indicate that the clouds remain in a cumulus-like state until CO_2 is lowered back to 400 ppmv. This strong hysteresis behavior is seen in both the LES and the bulk model.

To examine the cloud breakup and hysteresis further, we present two mechanism-denial experiments. First, shown in Figure 5, is a test for the influence of surface warming on cloud breakup.

This experiment follows the same protocol of sequentially increasing and then decreasing CO_2 concentration, but this time with SST and IS fixed to their 400 ppmv baseline values of 290 K and 8 K, respectively. In this experiment, the clouds do not break up even at CO_2 concentrations of

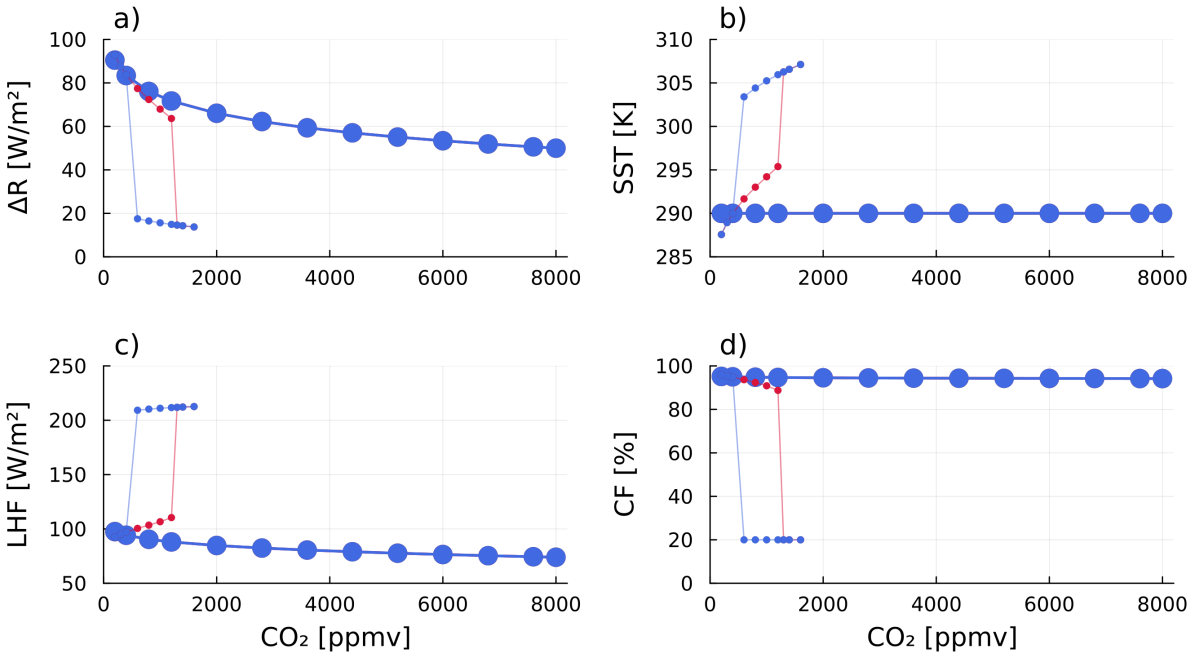

FIG. 5. Same as Figure 4, but with SST and inversion strength (IS) fixed at the 400 ppmv baseline values of 290 K and 8 K. Results from the fixed SST/IS experiment shown in large circles, with results from the slab ocean setup (Figure 4) shown by the small circles and thin lines. In the fixed SST/IS case, the CO_2 is varied from 200 ppmv to 8000 ppmv. Due to the stabilizing effect of fixing the SST, despite the suppression of cloud-top radiative cooling via the direct effect of CO_2, the stratocumulus clouds remain stable up to the extreme value of 8000 ppmv.

8000 ppmv. The radiative cooling continues to decrease, but so does the LHF as the boundary layer shallows and warms. This keeps the clouds relatively stable, with $\mathscr{D}$ only increasing up to around 0.4 at these very high CO_2 concentrations.

The second experiment, shown in Figure 6, tests the impact of the water vapor feedback on cloud breakup. This experiment is the same as the original, but now with the above-cloud water vapor concentrations seen by the radiation fixed at 2 g kg^{-1}. The above-cloud water vapor entrained into the cloud is still interactive and increases with SST. Because water vapor is a greenhouse gas and absorbs outgoing longwave radiation from the cloud tops, keeping it fixed mutes the

effect of increasing CO_2 and stabilizes the stratocumulus deck. Ultimately, the increasing CO_2 concentrations alone damp the cloud-top radiative cooling sufficiently to produce cloud breakup, but not until a concentration of 2800 ppmv is reached; this is nearly twice as much CO_2 as is required when the water vapor feedback is enabled. The hysteresis behavior is still seen, though the stratocumulus clouds do not reform until below 200 ppmv CO_2. The effect of radiative water vapor feedback thus is to shift the breakup threshold and broaden the hysteresis loop.

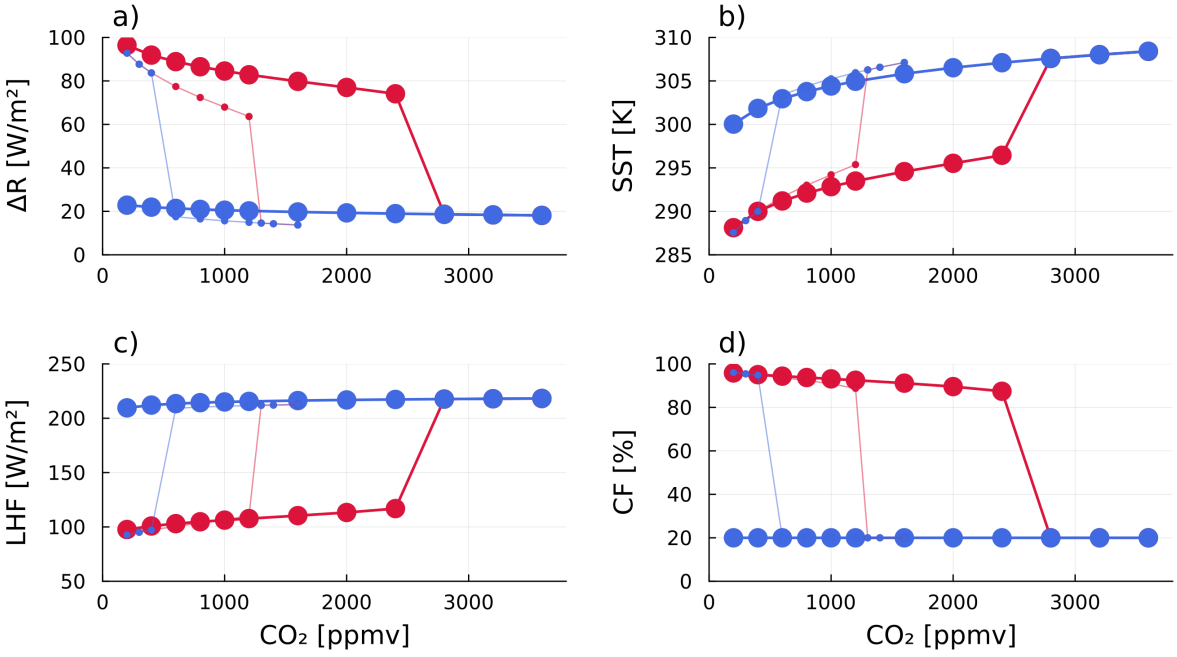

FIG. 6. Same as Figure 4, but with above-cloud water vapor concentrations shown to the radiation fixed at 2 g kg^{-1}. Above-cloud water vapor seen in the entrainment mixing remains interactive and increases with warming. Results from the fixed water vapor experiment shown in large circles, with results from the interactive setup (Figure 4) shown by the small circles and thin lines. In the fixed water vapor case, the CO_2 is varied from 200 ppmv to 4000 ppmv. The critical CO_2 threshold for cloud breakup is at 2800 ppmv.

The mechanisms discussed are summarized in the schematic in Figure 7. In our setup, CO_2 is the external control on the system and all other changes in large-scale conditions are parameterized. When CO_2 is increased, it directly reduces the cloud-top radiative cooling, ΔR. Smaller ΔR means the boundary layer is in a more decoupled state ($\mathscr{D}$ is around 3.5 after cloud breakup, or about 10x larger than at 400 ppmv). The cloud fraction is parameterized as a function of decoupling, so this decreases cloud cover. The first positive feedback, inherent to the system, is that cloud-top

cooling is proportional to cloud cover, $\Delta R = \mathrm{CF} \cdot f(\mathrm{CO_2}, \mathrm{H_2O})$ (Singer and Schneider (2023), their Eq. 8). This feedback is why the breakup is so rapid in $\mathrm{CO_2}$-space, as demonstrated, for example, in Figure 4 and along the stratocumulus-cumulus transition transect discussed in Singer and Schneider (2023).

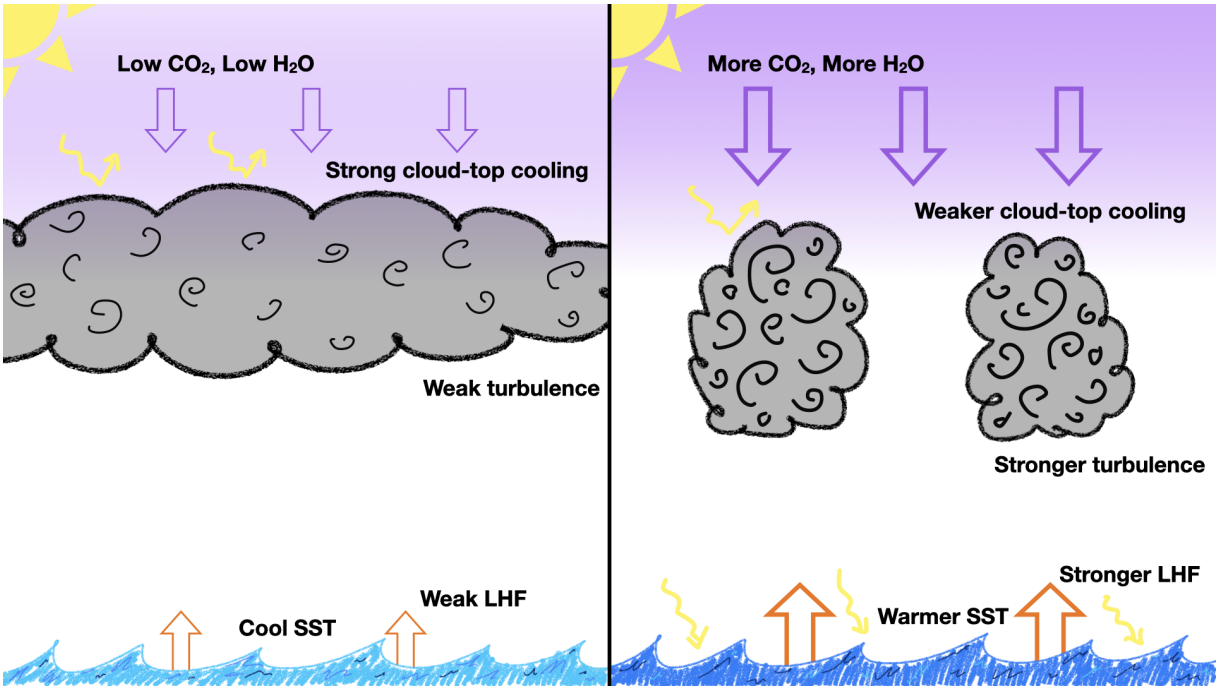

FIG. 7. Sketch showing important physical processes and positive feedbacks that contribute to stratocumulus breakup mechanisms. (Left) Low $\mathrm{CO_2}$ stratocumulus state. Low $\mathrm{CO_2}$ results in less downwelling radiation at the cloud top and strong cloud-top cooling. SSTs are lower because the high cloud cover blocks incoming shortwave radiation from reaching the surface and results in weak LHF and weak in-cloud turbulence. The combination of strong cloud-top cooling and weak LHF both contribute to strong coupling ($\mathscr{D}$ small). (Right) High $\mathrm{CO_2}$ cumulus state. More $\mathrm{CO_2}$ creates more downwelling radiation at cloud-top and weaker cloud-top cooling. This results in stronger decoupling, which reduces cloud fraction. Less cloud cover means more sunlight can reach the surface and warm it. Higher SSTs mean stronger LHF, which results in stronger turbulence in the cloud layer and further enhances decoupling. Higher temperatures also result in more above-cloud moisture, which further increases downwelling longwave radiation at cloud-top and weakens cloud-top cooling. The SST and water vapor feedbacks both act as positive feedbacks on the system.

The two mechanism-denial experiments above show the importance of the SST feedback and the radiative water vapor feedback. First, as cloud cover decreases, the ocean surface is exposed

to more sunlight and warms up. This increases SSTs and increases latent heat fluxes, which also contributes to stronger decoupling of the boundary layer. Second, as SSTs increase, the amount of water vapor in the free troposphere above the clouds also increases (water vapor feedback). Since water vapor is a greenhouse gas, like CO_2, more water vapor inhibits cloud-top radiative cooling, which decreases cloud cover further. As we saw above, the SST coupling is crucial in this bulk model for exhibiting stratocumulus breakup at any CO_2 concentration below 8000 ppmv; the water vapor feedback also contributes strongly to the stratocumulus breakup, reducing the critical CO_2 threshold from 2800 ppmv to 1300 ppmv.

However, neither this bulk model nor the LES from Schneider et al. (2019) can give robust quantitative information about the exact value of this critical CO_2 breakup threshold. Both models are sensitive to various parameter values and choices about how to couple the single stratocumulus box with the rest of the globe—e.g., how large-scale circulations and atmospheric stability might change with CO_2—which is necessarily parameterized in these setups.

b. Sensitivity of CO_2 breakup threshold to model parameters

Figure 8 shows the critical CO_2 stratocumulus breakup threshold as a function of the three parameters calibrated with EKI. The critical CO_2 concentration is calculated as the lowest CO_2 concentration for which the steady-state cloud fraction is less than 50% in a simulation of increasing CO_2. With the optimal parameter configuration shown in earlier results, the critical CO_2 threshold is at 1350 ppmv. For all three calibrated parameters, increasing parameter values results in a smaller critical CO_2 concentration. The critical value for cloud breakup is most sensitive to the surface exchange velocity, V, changing from 1900 ppmv to 750 ppmv for an 7% increase in V. For a large surface exchange velocity, the surface fluxes are larger for a given SST, meaning LHF will become untenably large at a lower SST and lead to cloud breakup. The ventilation coefficient (α_{vent}) dictates how much extra entrainment mixing results from cumulus updrafts in the decoupled state. As cloud fraction decreases and cumulus ventilation begins, stronger ventilation exacerbates decoupling by leading to clouds that occupy a smaller fraction of the boundary layer ($\mathscr{D} \propto (z_i - z_b)/z_i$). Therefore, stronger ventilation results in more rapid cloud breakup. Finally, the linearized surface shortwave cloud feedback is encoded in the b_{SW} term. When this radiation coefficient is larger, the surface

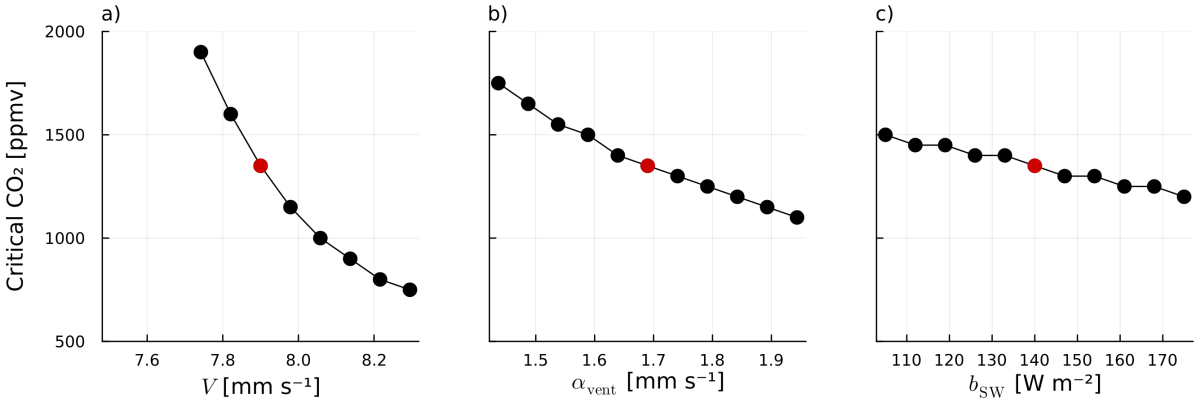

260 FIG. 8. Critical CO_2 threshold for stratocumulus breakup given different values of calibrated parameters: (a)
261 V surface exchange velocity, (b) α_{vent} entrainment ventilation mixing strength, and (c) b_{SW} shortwave cloud
262 feedback strength. Optimal parameter values shown in red.

277 heating resulting from cloud breakup is larger; hence, this also accelerates breakup and leads to a
278 smaller critical CO_2 value.

5. Conclusions

In this paper, we have highlighted the direct effect of CO_2 on stratocumulus clouds. These clouds, which are substantial contributors to the globally-averaged shortwave reflectance, are dynamically driven by cloud-top longwave radiative cooling. The radiative cooling creates negatively buoyant air at the cloud top, which sinks towards the surface, generates a convective overturning circulation, and resupplies the cloud layer with moisture. CO_2 (or infrared absorbers more generally, including water vapor and higher-altitude clouds) above the boundary layer reduce this radiative cooling and, at high enough concentrations, can decouple this overturning circulation from the moisture supply at the surface. This ultimately leads to the breakup of the cloud layer.

We have explored this mechanism of stratocumulus breakup with a conceptual bulk boundary layer model. Our model is forced by an externally prescribed CO_2 concentration and parameterizes all feedbacks (local surface warming and remote warming of the free troposphere) to predict the boundary layer thermodynamic and cloud properties. We have calibrated unconstrained parameters of the model such that it realistically reproduces behavior seen in LES from Schneider et al. (2019). With the bulk model, we can easily explore the importance of the local surface warming feedback and the water vapor feedback, which is linked to the remote warming in the tropics that controls free-tropospheric temperatures and water vapor concentrations. Because both local and remote surface warming, and hence water vapor concentrations in the free troposphere, increase with cloud cover reduction, there is strong hysteresis in the system: once the stratocumulus clouds break up, they will not reform again until CO_2 is lowered past the critical threshold at which they first broke up. The local surface warming will amplify the decoupling by increasing latent heat fluxes. And the remote surface warming and subsequent above-cloud water vapor increase will amplify decoupling by further reducing cloud-top cooling.

We have discussed the quantitative limitations of this model with regard to predicting the critical threshold of CO_2 for stratocumulus breakup. These limitations stem both from the simplicity of the representation of the subtropical cloud-topped boundary layer, as well as the simple representations of coupling between clouds and circulation. The threshold value is sensitive to parameter choices in our model, but the breakup and hysteresis behavior are robust and rooted in well understood physical principles.

The CO_2 direct effect, whereby cloud-top cooling is a mechanism for turbulence generation in the boundary layer, is included in some GCM parameterizations, but not in all (Qu et al. 2014). This neglect has implications for how GCMs respond to extreme CO_2 concentrations. These extreme concentrations are not relevant for 21st century climate change, but may be relevant for past climates; indeed, several studies suggest cloud feedbacks as a mechanism for enhanced warming in past climates (e.g., Zhu et al. 2019; Tierney et al. 2022). Furthermore, the direct effect of CO_2 on stratocumulus clouds introduces asymmetries and nonlinearities for deeper-time paleoclimate (Goldblatt et al. 2021) or future geoengineering scenarios (Schneider et al. 2020), where global cooling was, or could be, induced by solar dimming.

Acknowledgments. CES acknowledges support from NSF Graduate Research Fellowship under Grant No. DGE-1745301. This research was additionally supported by the generosity of Eric and Wendy Schmidt by recommendation of the Schmidt Futures program and by Charles Trimble. We thank Zhaoyi Shen for many helpful discussions in early stages of this project.

Data availability statement. The bulk model, along with examples reproducing all figures in this paper and documentation, is available on Github (`https://github.com/claresinger/MixedLayerModel.jl`).

References

Blossey, P. N., and Coauthors, 2013: Marine low cloud sensitivity to an idealized climate change: The CGILS LES intercomparison. *J. Adv. Model. Earth Syst.*, **5 (2)**, 234–258, https://doi.org/10.1002/jame.20025.

Bretherton, C. S., 2015: Insights into low-latitude cloud feedbacks from high-resolution models. *Philos. Trans. R. Soc. A Math. Phys. Eng. Sci.*, **373 (2054)**, https://doi.org/10.1098/rsta.2014.0415.

Bretherton, C. S., P. N. Blossey, and C. R. Jones, 2013: Mechanisms of marine low cloud sensitivity to idealized climate perturbations: A single-LES exploration extending the CGILS cases. *J. Adv. Model. Earth Syst.*, **5**, 316–337, https://doi.org/10.1002/jame.20019.

Bretherton, C. S., and M. C. Wyant, 1997: Moisture transport, lower-tropospheric stability, and decoupling of cloud-topped boundary layers. *J. Atmos. Sci.*, **54**, 148–167.

Brient, F., R. Roehrig, and A. Voldoire, 2019: Evaluating marine stratocumulus clouds in the CNRM-CM6-1 model using short-term hindcasts. *J. Adv. Model. Earth Syst.*, **11 (1)**, 127–148, https://doi.org/10.1029/2018MS001461.

Brient, F., and T. Schneider, 2016: Constraints on climate sensitivity from space-based measurements of low-cloud reflection. *J. Climate*, **29 (16)**, 5821–5835, https://doi.org/10.1175/JCLI-D-15-0897.1.

Ceppi, P., and P. Nowack, 2021: Observational evidence that cloud feedback amplifies global warming. *Proc. Natl. Acad. Sci.*, **118 (30)**, e2026290 118, https://doi.org/10.1073/pnas.2026290118.

Cesana, G. V., and A. D. Del Genio, 2021: Observational constraint on cloud feedbacks suggests moderate climate sensitivity. *Nat. Climate Change*, https://doi.org/10.1038/s41558-020-00970-y.

Christensen, M. W., G. G. Carrió, G. L. Stephens, and W. R. Cotton, 2013: Radiative impacts of free-tropospheric clouds on the properties of marine stratocumulus. *J. Atmos. Sci.*, **70 (10)**, 3102–3118, https://doi.org/10.1175/JAS-D-12-0287.1.

Dal Gesso, S., A. P. Siebesma, S. R. de Roode, and J. M. van Wessem, 2014: A mixed-layer model perspective on stratocumulus steady states in a perturbed climate. *Quart. J. Roy. Meteor. Soc.*, **140 (684)**, 2119–2131, https://doi.org/10.1002/qj.2282.

de Roode, S. R., A. P. Siebesma, S. Dal Gesso, H. J. J. Jonker, J. Schalkwijk, and J. Sival, 2014: A mixed-layer model study of the stratocumulus response to changes in large-scale conditions. *J. Adv. Model. Earth Syst.*, **6 (4)**, 1256–1270, https://doi.org/10.1002/2014MS000347.

Deardorff, J. W., 1980: Stratocumulus-capped mixed layers derived from a three-dimensional model. *Boundary-Layer Meteor.*, **18**, 495–527.

Dunbar, O. R. A., I. Lopez-Gomez, A. Garbuno-Iñigo, D. Z. Huang, E. Bach, and J.-l. Wu, 2022: EnsembleKalmanProcesses.jl: Derivative-free ensemble-based model calibration. *J. Open Source Software*, **7 (80)**, 4869, https://doi.org/10.21105/joss.04869.

Goldblatt, C., V. L. McDonald, and K. E. McCusker, 2021: Earth's long-term climate stabilized by clouds. *Nat. Geosci.*, https://doi.org/10.1038/s41561-021-00691-7.

Houtekamer, P. L., and F. Zhang, 2016: Review of the ensemble Kalman filter for atmospheric data assimilation. *Mon. Wea. Rev.*, **144**, 4489–4532.

Lee, H.-H., P. Bogenschutz, and T. Yamaguchi, 2022: Resolving away stratocumulus biases in modern global climate models. *Geophys. Res. Lett.*, https://doi.org/10.1029/2022GL099422.

Lilly, D. K., 1968: Models of cloud-topped mixed layers under a strong inversion. *Quart. J. Roy. Meteor. Soc.*, **94**, 292–309, https://doi.org/10.1002/qj.49709440106.

Lopez-Gomez, I., C. Christopoulos, H. L. Langeland Ervik, O. R. A. Dunbar, Y. Cohen, and T. Schneider, 2022: Training physics-based machine-learning parameterizations with gradient-free ensemble kalman methods. *J. Adv. Model. Earth Syst.*, **14 (8)**, e2022MS003 105, https://doi.org/10.1029/2022MS003105.

Miller, R. L., 1997: Tropical thermostats and low cloud cover. *J. Climate*, **10**, 409–440.

Myers, T. A., R. C. Scott, M. D. Zelinka, S. A. Klein, J. R. Norris, and P. M. Caldwell, 2021: Observational constraints on low cloud feedback reduce uncertainty of climate sensitivity. *Nat. Climate Change*, **11**, 501–507, https://doi.org/10.1038/s41558-021-01039-0.

Nam, C., S. Bony, J.-L. Dufresne, and H. Chepfer, 2012: The 'too few, too bright' tropical low-cloud problem in CMIP5 models. *Geophys. Res. Lett.*, **39 (21)**, https://doi.org/10.1029/2012GL053421.

Pierrehumbert, R. T., 1995: Thermostats, radiator fins, and the local runaway greenhouse. *J. Atmos. Sci.*, **52 (10)**, 1784–1806, https://doi.org/10.1175/1520-0469(1995)052<1784:TRFATL>2.0.CO;2.

Qu, X., A. Hall, S. A. Klein, and P. M. Caldwell, 2014: On the spread of changes in marine low cloud cover in climate model simulations of the 21st century. *Climate Dynamics*, **42 (9-10)**, 2603–2626, https://doi.org/10.1007/s00382-013-1945-z.

Raghuraman, S. P., D. Paynter, and V. Ramaswamy, 2021: Anthropogenic forcing and response yield observed positive trend in Earth's energy imbalance. *Nat. Comm.*, **12 (1)**, 1–10, https://doi.org/10.1038/s41467-021-24544-4.

Schillings, C., and A. M. Stuart, 2017: Analysis of the ensemble Kalman filter for inverse problems. *SIAM J. Numer. Anal.*, **55**, 1264–1290.

Schneider, T., C. M. Kaul, and K. G. Pressel, 2019: Possible climate transitions from breakup of stratocumulus decks under greenhouse warming. *Nat. Geosci.*, **12 (3)**, 163–167, https://doi.org/10.1038/s41561-019-0310-1.

Schneider, T., C. M. Kaul, and K. G. Pressel, 2020: Solar geoengineering may not prevent strong warming from direct effects of CO_2 on stratocumulus cloud cover. *Proc. Natl. Acad. Sci.*, **117 (48)**, 30 179–30 185, https://doi.org/10.1073/pnas.2003730117.

Schneider, T., J. Teixeira, C. S. Bretherton, F. Brient, K. G. Pressel, C. Schär, and A. P. Siebesma, 2017: Climate goals and computing the future of clouds. *Nat. Climate Change opinion & comment*, **7 (1)**, 3–5, https://doi.org/10.1038/nclimate3190.

Sherwood, S. C., and Coauthors, 2020: An assessment of Earth's climate sensitivity using multiple lines of evidence. *Rev. of Geophysics*, **58 (4)**, e2019RG000 678, https://doi.org/10.1029/2019RG000678.

Singer, C. E., and T. Schneider, 2023: Stratocumulus-cumulus transition explained by bulk boundary layer theory. *J. Climate*, https://doi.org/tbd-a.

Stevens, B., 2006: Bulk boundary-layer concepts for simplified models of tropical dynamics. *Theor. Comput. Fluid Dyn.*, **20 (5-6)**, 279–304, https://doi.org/10.1007/s00162-006-0032-z.

Tan, Z., T. Schneider, J. Teixeira, and K. G. Pressel, 2017: Large-eddy simulation of subtropical cloud-topped boundary layers: 2. Cloud response to climate change. *J. Adv. Model. Earth Sys.*, **9**, 19–38.

Tierney, J. E., and Coauthors, 2022: Spatial patterns of climate change across the Paleocene–Eocene Thermal Maximum. *Proc. Natl. Acad. Sci.*, **119 (42)**, e2205326 119, https://doi.org/10.1073/pnas.2205326119.

Zelinka, M. D., S. A. Klein, Y. Qin, and T. A. Myers, 2022: Evaluating climate models' cloud feedbacks against expert judgment. *J. Geophys. Research: Atmospheres*, **127 (2)**, e2021JD035 198, https://doi.org/10.1029/2021JD035198.

Zhang, M., C. S. Bretherton, P. N. Blossey, S. Bony, F. Brient, and J.-C. Golaz, 2012: The CGILS experimental design to investigate low cloud feedbacks in general circulation models

by using single-column and large-eddy simulation models. *J. Adv. Model. Earth Syst.*, **4**, 1–15, https://doi.org/10.1029/2012MS000182.

Zhu, J., C. J. Poulsen, and J. E. Tierney, 2019: Simulation of Eocene extreme warmth and high climate sensitivity through cloud feedbacks. *Science Advances*, **5 (9)**, eaax1874, https://doi.org/10.1126/sciadv.aax1874, 31555736.